Mathematical Biosciences and Engineering

https://www.aimspress.com/journal/mbe

MBE, 23(8): 2489–2515.
DOI: 10.3934/mbe.2026091
Received: 09 June 2026
Revised: 19 July 2026
Accepted: 10 August 2026
Published: 18 August 2026

Research article

A reaction–diffusion delay model for spatial tumor virotherapy with optimal control

Fathalla A. Rihan*

Department of Mathematical Sciences, College of Science, UAE University, Al-Ain, 15551, UAE

* **Correspondence:** Email: frihan@uaeu.ac.ae; Tel: +97137136392.

Abstract: Oncolytic virotherapy uses viruses that selectively infect and lyse tumor cells while promoting antitumor immunity. Because viral spread, tumor growth, and immune-cell migration are spatially heterogeneous, purely temporal models may miss important treatment dynamics. We develop a reaction–diffusion delay model for spatial tumor virotherapy with a virus-induced cytotoxic T-lymphocyte (CTL) response, thereby incorporating tumor growth, infection, lysis, immune-mediated killing, diffusion, and delayed immune activation. We prove positivity, local well-posedness, and global boundedness under explicit sufficient conditions, and analyze spatially homogeneous equilibria and modal stability. Then, we extend the model with a numerical optimal-control formulation for viral administration and immune stimulation, thus minimizing tumor burden, treatment cost, and excessive CTL proliferation. Simulations indicate that tumor–virus–immune dynamics can remain spatially heterogeneous and that the computed optimal control schedules improve tumor suppression for the chosen parameter set.

Keywords: oncolytic virotherapy; tumor–virus interaction; cytotoxic T lymphocytes; reaction–diffusion equations; delay differential equations; optimal control

1. Introduction

Cancer remains a major global health challenge, motivating the development of therapeutic strategies that improve tumor control and long-term survival. Oncolytic virotherapy is a promising anticancer approach in which viruses selectively infect, replicate within, and destroy tumor cells while causing limited damage to healthy tissue [1–4]. Viral replication leads to tumor-cell lysis and the release of progeny virions, thus allowing the infection to spread to neighboring tumor cells and generate a self-amplifying antitumor effect.

Oncolytic viruses can also stimulate antitumor immunity. Viral infection induces immunogenic tumor-cell death, enhances antigen presentation, remodels the tumor microenvironment, and promotes tumor-specific cytotoxic T-lymphocyte (CTL) responses [5–7]. Therefore, treatment outcomes depend

not only on direct viral oncolysis but also on the interactions among uninfected tumor cells, infected tumor cells, free virus particles, and immune effector cells. The main biological mechanisms are illustrated in Figure 1.

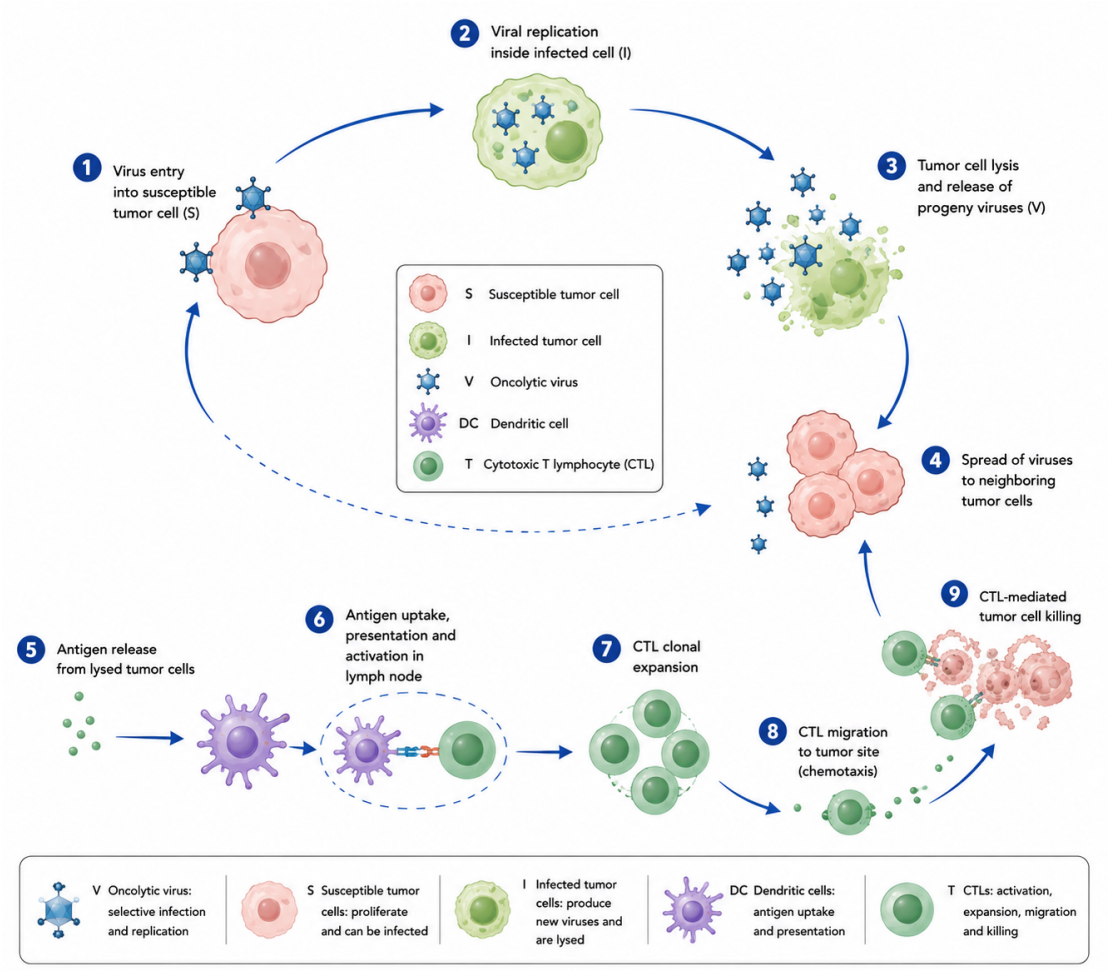

Figure 1. Schematic illustration of oncolytic virotherapy. Viruses V infect susceptible tumor cells S, producing infected cells I. Viral replication induces cell lysis and antigen release, which activate CTL-mediated tumor-cell killing by T.

Mathematical models provide useful tools to investigate the nonlinear mechanisms underlying tumor virotherapy. Tumor–virus–immune interactions have been described using ordinary differential equations, delay differential equations, nonlocal models, fractional-order systems, and reaction–diffusion equations [8–11]. Delay terms are particularly important because immune activation is not instantaneous. Antigen release, antigen presentation, immune priming, CTL expansion, and migration toward the tumor all require time [12, 13]. Such delays may substantially affect transient behavior, stability, and oscillatory tumor–virus–immune dynamics.

Spatial effects are equally important. Within a heterogeneous tumor microenvironment, tumor cells, virus particles, and immune cells are nonuniformly distributed. Viruses spread from infected regions, immune cells migrate toward sites of antigenic stimulation, and tumor cells proliferate at spatially varying rates. Consequently, purely temporal models may fail to capture infection fronts, heterogeneous

immune infiltration, and spatially dependent treatment responses. Reaction–diffusion models provide a natural framework to incorporate these mechanisms and to study the interaction between spatial transport and delayed immune activation [14–17].

Motivated by these considerations, we formulate a reaction–diffusion delay model for virus-induced tumor-specific immune responses. The model extends the temporal delay framework of Li and Xiao [11] by incorporating spatial diffusion of uninfected tumor cells, virus-infected tumor cells, free virus particles, and tumor-specific CTLs. Recent studies have shown that diffusion, nonlocal effects, and virus-induced immune signaling can strongly influence virotherapy outcomes [18–22].

Previous mathematical studies have investigated temporal delay models for virus-induced tumor-specific immune responses [11], spatial formulations with nonlocal diffusion [20], and optimal-control approaches to tumor immunotherapies [23]. The present work develops a unified spatial-delay framework that links viral spread, delayed CTL activation, and treatment scheduling. Specifically, we accomplish the following:

1) formulate a reaction–diffusion delay model for tumor–virus–CTL interactions;
2) establish positivity, local well-posedness, and global boundedness under explicit sufficient conditions;
3) derive the characteristic equation associated with each spatial mode;
4) develop a direct numerical optimal-control extension for viral dosing and immune stimulation.

Global existence and uniform boundedness are obtained under an explicit sufficient parameter condition requiring CTL clearance to dominate the maximal tumor-induced CTL proliferation rate. Analytical conclusions are separately stated from numerical observations, which are restricted to the selected scaled parameter set.

The remainder of the paper is organized as follows: Section 2 introduces the model, initial and boundary conditions, positivity, boundedness, equilibria, and invasion thresholds; Section 3 develops the spatial-mode stability framework; Section 4 presents the continuous optimal-control formulation, the formal optimality conditions, and the semi-discrete numerical implementation; Section 5 provides the numerical simulations; finally, Sections 6 and 7 contain the discussion and concluding remarks.

2. Model formulation and biological interpretation

Let $\Omega \subset \mathbb{R}^n$, $n \geq 1$, represent the tumor region, with sufficiently smooth boundaries $\partial\Omega$. Let $x \in \Omega$ represent the spatial location, and $t > 0$ represent time. We define $S(x,t)$, $I(x,t)$, $V(x,t)$, and $T(x,t)$ as densities of uninfected tumor cells, infected tumor cells, oncolytic virus particles, and tumor-specific cytotoxic T lymphocytes, respectively. The proposed reaction–diffusion delay model is as follows:

$$\begin{cases} \dfrac{\partial S}{\partial t} = D_S \Delta S + rS\left(1 - \dfrac{S+I}{K}\right) - \beta S V - \alpha S T, \\ \dfrac{\partial I}{\partial t} = D_I \Delta I + \beta S V - \delta I - \alpha I T, \\ \dfrac{\partial V}{\partial t} = D_V \Delta V + b\delta I - \mu V, \\ \dfrac{\partial T}{\partial t} = D_T \Delta T + \mathcal{G}(V_\tau, T_\tau) + \gamma(S+I)T - dT. \end{cases} \tag{2.1}$$

Δ represents the Laplace operator with respect to the spatial variable (x). The diffusion terms $D_S\Delta S$, $D_I\Delta I$, $D_V\Delta V$, and $D_T\Delta T$ describe spatial movement of the corresponding populations; zero diffusion indicates spatial immobility. The model structure is illustrated in Figure 2.

The delayed nonlinear term

$$\mathcal{G}(V_\tau, T_\tau) := \frac{cV(x,t-\tau)T(x,t-\tau)}{1+h_1V(x,t-\tau)+h_2T(x,t-\tau)}$$

models virus-induced CTL activation after a finite immune response time $\tau > 0$.

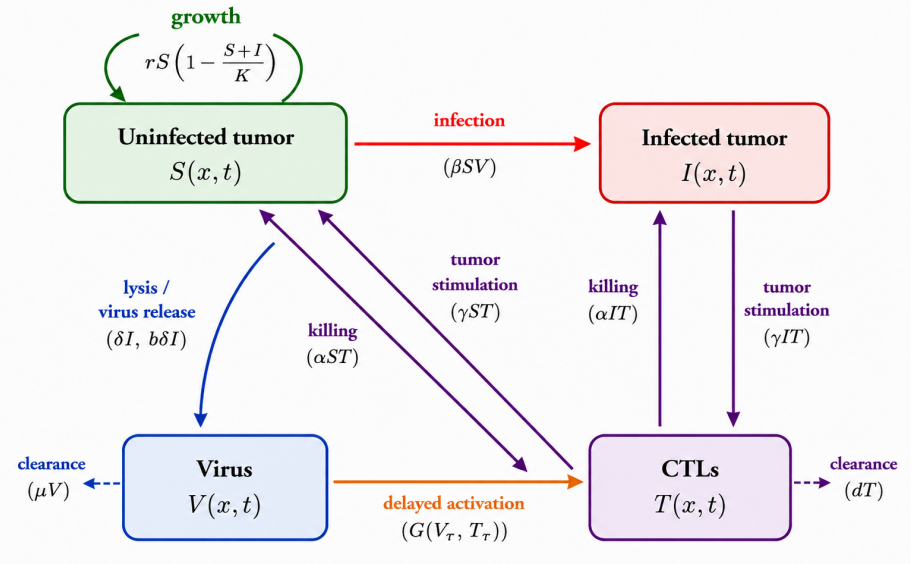

Figure 2. Schematic of the reaction–diffusion delay model. Both uninfected and infected tumor cells stimulate the CTL response through the term $\gamma(S+I)T$, whereas CTLs mediate the killing of both tumor-cell populations. Infected tumor-cell lysis leads to virus release, while virus-induced CTL activation occurs after a time delay. The terms $D_S\Delta S$, $D_I\Delta I$, $D_V\Delta V$, and $D_T\Delta T$ represent spatial movement of the corresponding populations.

The first equation in (2.1) describes uninfected tumor cells. The term $rS\left(1-\frac{S+I}{K}\right)$ represents logistic tumor growth, where r is the intrinsic tumor proliferation rate, and K is the carrying capacity. The total tumor burden is represented by $S+I$. The term βSV describes the infection of uninfected tumor cells by free oncolytic viruses, while αST represents the immune-mediated killing of uninfected tumor cells by tumor-specific cytotoxic T lymphocytes.

The second equation describes infected tumor cells. These cells are generated through viral infection at a rate of βSV. They are removed through viral lysis at a rate of δI and through immune-mediated killing at a rate of αIT.

The third equation models free oncolytic virus particles. Virus particles are produced from lysed infected tumor cells at a rate of $b\delta I$, where b is the viral burst size. Free virus particles are cleared at a rate of μV.

The fourth equation describes the cytotoxic T-lymphocyte response to the tumor. The time delay $\tau > 0$ represents the biological time required for infected tumor cells to release antigens and danger signals, activate tumor-specific T cells, and allow the expanded CTL population to become active within

the tumor microenvironment. In the numerator of the delayed response term, the past virus concentration and CTL population jointly promote CTL proliferation, whereas the denominator accounts for saturation due to viral stimulation and competition among CTLs. The parameter c represents the virus-induced CTL proliferation coefficient, h_1 measures saturation with respect to viral stimulation, and h_2 measures CTL competition.

Table 1. Description of the parameters in the reaction–diffusion delay model.

Parameter	Biological meaning
D_S	Diffusion coefficient of uninfected tumor cells
D_I	Diffusion coefficient of infected tumor cells
D_V	Diffusion coefficient of oncolytic virus particles
D_T	Diffusion coefficient of tumor-specific CTLs
r	Intrinsic proliferation rate of tumor cells
K	Tumor carrying capacity
β	Infection rate of tumor cells by oncolytic viruses
α	Killing rate of tumor cells by tumor-specific CTLs
δ	Lysis rate of infected tumor cells
b	Viral burst size
μ	Clearance rate of free oncolytic viruses
c	Virus-induced CTL proliferation coefficient
h_1	Saturation parameter for viral activation of CTLs
h_2	Competition parameter among CTLs
γ	Tumor-induced CTL stimulation rate
d	Clearance rate of tumor-specific CTLs
τ	Activation delay of the virus-induced CTL response

The term $\gamma(S+I)T$ represents tumor-antigen-driven CTL stimulation. It assumes that CTL expansion or activation is proportional to both the total tumor burden $S+I$ and the existing CTL population T, thereby providing a mass-action approximation of repeated CTL interactions with tumor-associated antigens. This term does not distinguish between the potentially different immunogenicities of uninfected and virus-infected tumor cells, which is a limitation of the model. The term dT represents natural CTL clearance.

In the tumor microenvironment, spatial movement is represented by diffusion terms. In particular, $D_V\Delta V$ describes the spatial spread of virus particles, $D_T\Delta T$ represents CTL migration, and $D_S\Delta S$ and $D_I\Delta I$ describe the local movement of uninfected and infected tumor cells, respectively. For compact notation, define

$$U=(S,I,V,T)^{\top},\quad U_\tau(x,t)=U(x,t-\tau),\ \text{and}\ \mathcal{D}=\operatorname{diag}(D_S,D_I,D_V,D_T).$$

Then (2.1) may be written as follows:

$$\frac{\partial U}{\partial t}=\mathcal{D}\Delta U+\mathcal{F}(U,U_\tau). \tag{2.2}$$

The model parameters and their biological meanings are summarized in Table 1.

2.1. Initial and boundary conditions

Because model (2.1) contains a discrete time delay, the initial data must be prescribed as history functions on $[-\tau, 0]$. We assume

$$S(x,\theta) = \phi_S(x,\theta), \quad I(x,\theta) = \phi_I(x,\theta), \quad V(x,\theta) = \phi_V(x,\theta), \quad T(x,\theta) = \phi_T(x,\theta), \tag{2.3}$$

for $x \in \Omega$ and $\theta \in [-\tau, 0]$, where

$$\phi_S, \phi_I, \phi_V, \phi_T \geq 0. \tag{2.4}$$

The nonnegativity of the history functions is biologically necessary because the state variables represent densities.

For a closed tumor region, homogeneous Neumann boundary conditions are imposed:

$$\frac{\partial S}{\partial n} = \frac{\partial I}{\partial n} = \frac{\partial V}{\partial n} = \frac{\partial T}{\partial n} = 0, \quad x \in \partial\Omega, \quad t > 0, \tag{2.5}$$

where $\partial/\partial n$ denotes differentiation in the outward normal direction on $\partial\Omega$. These conditions imply that tumor cells, infected cells, virus particles, and CTLs do not cross the boundary of the tumor region.

2.2. Local well-posedness and nonnegativity

Proposition 2.1 (Local well-posedness)**.** *Let $\Omega \subset \mathbb{R}^n$ be bounded with a sufficiently smooth boundary, and assume that all parameters are nonnegative, with $K, \delta, \mu, d > 0$. Let*

$$X = C(\overline{\Omega}; \mathbb{R}^4), \quad \phi = (\phi_S, \phi_I, \phi_V, \phi_T) \in C([-\tau, 0]; X_+),$$

where X_+ denotes the nonnegative cone of X. Then, there exists $t_{\max} > 0$ and a unique mild solution of (2.1)–(2.5) *on $[-\tau, t_{\max})$ which satisfy the following:*

$$U(\theta) = \phi(\theta), \quad -\tau \leq \theta \leq 0.$$

If $t_{\max} < \infty$, then

$$\limsup_{t \uparrow t_{\max}} \|U_t\|_{C([-\tau,0];X)} = \infty,$$

where $U_t(\theta) = U(t+\theta)$. Consequently, if the history norm $\|U_t\|_{C([-\tau,0];X)}$ remains bounded on every bounded time interval, then the solution can be continued.

Proof. The diagonal Neumann diffusion operator

$$\mathcal{A} = \mathrm{diag}(D_S\Delta, D_I\Delta, D_V\Delta, D_T\Delta)$$

generates an analytic positive semigroup on X. For every nonnegative history,

$$1 + h_1\psi_V(x,-\tau) + h_2\psi_T(x,-\tau) \geq 1$$

Hence, in a sufficiently small open neighborhood of any nonnegative history, the denominator in the delayed activation term remains bounded away from zero. Therefore, the reaction mapping therefore extends to a locally Lipschitz mapping on that neighborhood. Then, the standard theory for semilinear parabolic functional differential equations then yields a unique local mild solution and the usual continuation alternative; see [24–27]. □

The following result states the basic invariance property of the nonnegative cone.

Proposition 2.2 (Nonnegativity)**.** *Under the assumptions of Proposition 2.1, the mild solution remains nonnegative throughout its interval of existence:*

$$S(x,t),\ I(x,t),\ V(x,t),\ T(x,t) \geq 0, \quad x \in \overline{\Omega}, \quad 0 \leq t < t_{\max}.$$

Proof. Let $\psi \in C([-\tau, 0]; X_+)$ be a nonnegative history. The reaction mapping is quasi-positive. Indeed, for each $x \in \overline{\Omega}$,

$$\psi_S(x,0) = 0 \quad \Longrightarrow \quad \mathcal{F}_S(\psi)(x) = 0,$$

$$\psi_I(x,0) = 0 \quad \Longrightarrow \quad \mathcal{F}_I(\psi)(x) = \beta\psi_S(x,0)\psi_V(x,0) \geq 0,$$

$$\psi_V(x,0) = 0 \quad \Longrightarrow \quad \mathcal{F}_V(\psi)(x) = b\delta\psi_I(x,0) \geq 0,$$

and

$$\psi_T(x,0) = 0 \quad \Longrightarrow \quad \mathcal{F}_T(\psi)(x) = \frac{c\,\psi_V(x,-\tau)\psi_T(x,-\tau)}{1 + h_1\psi_V(x,-\tau) + h_2\psi_T(x,-\tau)} \geq 0.$$

Thus, on every boundary face of the nonnegative cone, the corresponding reaction component points inward or is tangent to the boundary. Positivity of the Neumann semigroup, together with the invariance principle for semilinear parabolic delay equations, implies that X_+ is invariant. Hence, the mild solution remains nonnegative on $[0, t_{\max})$; see [26, 27]. □

The following result provides an explicit parameter regime under which the local solution is global and uniformly bounded. Biologically, the condition requires natural CTL clearance to dominate the maximal tumor-induced CTL proliferation, while the delayed virus-induced activation remains bounded because of saturation.

Theorem 2.3 (Global existence and uniform boundedness)**.** *Assume the hypotheses of Proposition 2.1 and, in addition, suppose that*

$$D_S = D_I =: D_N, \quad h_2 > 0, \quad d > \gamma M_N,$$

where

$$M_N := \max\left\{K,\ \|\phi_S + \phi_I\|_{L^\infty(\overline{\Omega}\times[-\tau,0])}\right\}.$$

Then the nonnegative solution of (2.1)–(2.5) *exists for all $t \geq 0$ and remains uniformly bounded. More precisely, define*

$$M_V := \max\left\{\|\phi_V\|_{L^\infty(\overline{\Omega}\times[-\tau,0])},\ \frac{b\delta M_N}{\mu}\right\}.$$

Then

$$0 \leq S(x,t) + I(x,t) \leq M_N, \quad 0 \leq V(x,t) \leq M_V,$$

and

$$0 \leq T(x,t) \leq \max\left\{\|\phi_T\|_{L^\infty(\overline{\Omega}\times[-\tau,0])},\ \frac{cM_V}{h_2(d - \gamma M_N)}\right\}$$

for all $x \in \overline{\Omega}$ and $t \geq 0$. Consequently, S, I, V, and T are uniformly bounded.

Proof. Set $N = S + I$. Since $D_S = D_I = D_N$, adding the first two equations of (2.1) gives the following:

$$N_t - D_N \Delta N = rS\left(1 - \frac{N}{K}\right) - \delta I - \alpha NT.$$

At any first point where N reaches a value greater than or equal to M_N, one has $N \geq K$, and hence

$$rS\left(1 - \frac{N}{K}\right) - \delta I - \alpha NT \leq 0.$$

Therefore, the parabolic maximum principle therefore gives the following:

$$0 \leq N(x,t) \leq M_N.$$

Since $S, I \geq 0$, it follows that

$$0 \leq S(x,t),\ I(x,t) \leq M_N.$$

The virus equation satisfies

$$V_t - D_V \Delta V \leq b\delta M_N - \mu V.$$

Then, a comparison argument yields

$$0 \leq V(x,t) \leq M_V.$$

For the delayed CTL activation term, positivity and $h_2 > 0$ imply

$$0 \leq \frac{cV(x,t-\tau)T(x,t-\tau)}{1 + h_1 V(x,t-\tau) + h_2 T(x,t-\tau)} \leq \frac{c}{h_2} V(x,t-\tau) \leq \frac{cM_V}{h_2}.$$

Moreover, $S + I \leq M_N$, and therefore,

$$T_t - D_T \Delta T \leq \frac{cM_V}{h_2} - (d - \gamma M_N)T.$$

Since $d - \gamma M_N > 0$, comparison with the corresponding scalar linear equation gives the following:

$$T(x,t) \leq \max\left\{\|\phi_T\|_{L^\infty(\overline{\Omega}\times[-\tau,0])}, \frac{cM_V}{h_2(d - \gamma M_N)}\right\}.$$

Thus, all state variables remain uniformly bounded. Then, the continuation criterion in Proposition 2.1 then implies global existence. □

Remark 2.4 (Biological interpretation)**.** *The condition $d > \gamma M_N$ is sufficient but not necessary. It requires CTL clearance to exceed the largest tumor-induced CTL proliferation rate allowed by the tumor bound. The delayed virus-induced activation cannot cause unbounded growth because the term $h_2 T(x, t-\tau)$ saturates the CTL response. For the baseline uncontrolled parameter set,*

$$D_S = D_I, \quad M_N = K = 1, \quad d = 0.42 > \gamma M_N = 0.30,$$

so the theorem applies.

2.3. Spatially homogeneous equilibria

The spatially homogeneous equilibria of (2.1) coincide with those of the corresponding delay differential equation model because all diffusion terms vanish for spatially homogeneous solutions. At an equilibrium, the delay also disappears because

$$V(x, t-\tau) = V^*, \quad T(x, t-\tau) = T^*.$$

Thus, the equilibria satisfy

$$\begin{cases} 0 = rS\left(1 - \dfrac{S+I}{K}\right) - \beta S V - \alpha S T, \\ 0 = \beta S V - \delta I - \alpha I T, \\ 0 = b\delta I - \mu V, \\ 0 = \dfrac{cVT}{1 + h_1 V + h_2 T} + \gamma(S+I)T - dT. \end{cases} \tag{2.6}$$

Proposition 2.5 (Boundary equilibria)**.** *System* (2.1) *admits the tumor-free equilibrium*

$$E_0 = (0, 0, 0, 0)$$

and the virus-free, immune-free tumor equilibrium

$$E_1 = (K, 0, 0, 0).$$

Define the following:

$$\mathcal{R}_0 = \frac{bK\beta}{\mu}. \tag{2.7}$$

If $\mathcal{R}_0 > 1$*, then immune-free persistent-virus equilibrium*

$$E_2 = (S_2, I_2, V_2, 0) \tag{2.8}$$

exists, where

$$S_2 = \frac{\mu}{b\beta}, \quad I_2 = \frac{r\mu(bK\beta - \mu)}{b\beta(bK\delta\beta + r\mu)}, \quad V_2 = \frac{r\delta(bK\beta - \mu)}{\beta(bK\delta\beta + r\mu)}.$$

If $d/(\gamma K) < 1$*, the virus-free immune equilibrium*

$$E_3 = \left(\frac{d}{\gamma}, 0, 0, \frac{r}{\alpha}\left(1 - \frac{d}{\gamma K}\right)\right) \tag{2.9}$$

is biologically feasible.

Proof. Setting the diffusion and time-derivative terms equal to zero in (2.1) gives the equilibrium system. The equilibria E_0 and E_1 follow directly. Setting $T = 0$ and solving the remaining algebraic equations gives E_2; its positive components require $bK\beta - \mu > 0$, equivalently $\mathcal{R}_0 > 1$. Setting $I = V = 0$ gives E_3, whose CTL component is positive precisely when $d/(\gamma K) < 1$. □

A fully positive equilibrium $E^* = (S^*, I^*, V^*, T^*)$ satisfies (2.6) with all components positive. From the third equilibrium equation,

$$I^* = \frac{\mu}{b\delta} V^*. \tag{2.10}$$

The remaining equilibrium equations reduce to algebraic equations for S^*, V^*, and T^*. The existence of a positive equilibrium depends on the viral infection capacity, immune activation strength, and tumor carrying capacity.

2.4. Invasion thresholds at boundary equilibria

Proposition 2.6 (Boundary-equilibrium invasion thresholds)**.** *Assume that $r > 0$. Then, E_0 is linearly unstable.*

At E_1, viral and CTL invasion are both excluded if

$$\mathcal{R}_0 < 1, \quad \gamma K < d.$$

Viral invasion occurs if $\mathcal{R}_0 > 1$, whereas CTL invasion occurs if $\gamma K > d$.

At E_2, CTL invasion through the spatially homogeneous mode occurs if

$$\frac{cV_2}{1 + h_1 V_2} + \gamma(S_2 + I_2) > d.$$

If $E_3 = (S_3, 0, 0, T_3)$ exists, define

$$\mathcal{R}_V^{(3)} = \frac{b\delta\beta S_3}{\mu(\delta + \alpha T_3)}.$$

Then, the infected-cell–virus subsystem is resistant to invasion in all spatial modes when $\mathcal{R}_V^{(3)} < 1$. If $\mathcal{R}_V^{(3)} > 1$, then the spatially homogeneous mode is unstable to viral invasion. The threshold cases in which equality holds are not considered here.

Proof. At E_0, the eigenvalue associated with the spatially homogeneous susceptible-tumor perturbation is $r > 0$; hence, E_0 is linearly unstable.

At E_1, linearization of the infected-cell–virus subsystem gives the threshold $\mathcal{R}_0$, while the CTL perturbation has an eigenvalue of $\gamma K - d$. This yields the stated viral- and CTL-invasion conditions.

At E_2, the spatially homogeneous CTL perturbation satisfies

$$\dot{w}(t) = [\gamma(S_2 + I_2) - d]w(t) + \frac{cV_2}{1 + h_1 V_2} w(t - \tau).$$

Its characteristic equation is

$$\lambda = \gamma(S_2 + I_2) - d + \frac{cV_2}{1 + h_1 V_2} e^{-\lambda\tau}.$$

If

$$\frac{cV_2}{1 + h_1 V_2} + \gamma(S_2 + I_2) - d > 0,$$

then, the characteristic equation has a positive real root, and hence CTL invasion occurs.

Finally, linearizing the infected-cell–virus subsystem at E_3 gives the following:

$$\begin{pmatrix} \dot{i} \\ \dot{v} \end{pmatrix} = \begin{pmatrix} -(\delta + \alpha T_3) & \beta S_3 \\ b\delta & -\mu \end{pmatrix} \begin{pmatrix} i \\ v \end{pmatrix}.$$

The trace is negative, while the determinant is

$$\mu(\delta + \alpha T_3) - b\delta\beta S_3.$$

Therefore, the homogeneous subsystem is stable when $\mathcal{R}_V^{(3)} < 1$ and unstable when $\mathcal{R}_V^{(3)} > 1$. For nonzero spatial modes, diffusion adds nonnegative quantities to the magnitudes of the diagonal losses, so it cannot destabilize this invasion subsystem when the homogeneous mode is stable. □

3. Linearization and modal stability analysis

Let

$$E^* = (S^*, I^*, V^*, T^*)$$

be a spatially homogeneous positive equilibrium of system (2.1). We introduce perturbations

$$S = S^* + s, \quad I = I^* + i, \quad V = V^* + v, \quad T = T^* + w,$$

and write $Z = (s, i, v, w)^\top$. The linearized system has the form

$$\frac{\partial Z}{\partial t} = D\Delta Z + AZ(x,t) + BZ(x,t-\tau), \tag{3.1}$$

where

$$D = \operatorname{diag}(D_S, D_I, D_V, D_T).$$

The instantaneous Jacobian matrix is

$$A = \begin{pmatrix} a_{11} & a_{12} & a_{13} & a_{14} \\ a_{21} & a_{22} & a_{23} & a_{24} \\ 0 & b\delta & -\mu & 0 \\ \gamma T^* & \gamma T^* & 0 & \gamma(S^* + I^*) - d \end{pmatrix}, \tag{3.2}$$

with

$$a_{11} = r\left(1 - \frac{2S^* + I^*}{K}\right) - \beta V^* - \alpha T^*, \quad a_{12} = -\frac{rS^*}{K},$$

$$a_{13} = -\beta S^*, \quad a_{14} = -\alpha S^*,$$

$$a_{21} = \beta V^*, \quad a_{22} = -\delta - \alpha T^*, \quad a_{23} = \beta S^*, \quad a_{24} = -\alpha I^*.$$

The delayed term appears only in the CTL equation, so

$$B = \begin{pmatrix} 0 & 0 & 0 & 0 \\ 0 & 0 & 0 & 0 \\ 0 & 0 & 0 & 0 \\ 0 & 0 & b_{43} & b_{44} \end{pmatrix}, \tag{3.3}$$

where

$$b_{43} = \frac{cT^*(1 + h_2 T^*)}{(1 + h_1 V^* + h_2 T^*)^2}, \quad b_{44} = \frac{cV^*(1 + h_1 V^*)}{(1 + h_1 V^* + h_2 T^*)^2}.$$

Let ρ_k, $k = 0, 1, 2, \ldots$, be the Neumann eigenvalues of $-\Delta$, ordered as $0 = \rho_0 < \rho_1 \le \rho_2 \le \cdots$, with corresponding eigenfunctions ϕ_k. Seeking modal solutions

$$Z(x,t) = e^{\lambda t} q \phi_k(x), \quad q \in \mathbb{C}^4, \quad q \neq 0,$$

gives the modal characteristic equation

$$\det\left[\lambda I_4 + \rho_k D - A - Be^{-\lambda\tau}\right] = 0, \quad k = 0, 1, 2, \ldots. \tag{3.4}$$

The mode $k = 0$ represents spatially homogeneous perturbations, while $k \ge 1$ represents spatially heterogeneous perturbations.

Theorem 3.1 (Modal stability criterion)**.** *If, for every $k = 0, 1, 2, \ldots$, all roots of (3.4) satisfy*

$$\mathrm{Re}(\lambda) < 0,$$

then E^* is locally asymptotically stable with respect to small spatially dependent perturbations satisfying the homogeneous Neumann boundary condition. If, for some $k \ge 0$, Equation (3.4) has a root with

$$\mathrm{Re}(\lambda) > 0,$$

then E^* is linearly unstable.

Proof. Expanding

$$Z(x,t) = \sum_{k=0}^{\infty} z_k(t)\phi_k(x)$$

and using $-\Delta\phi_k = \rho_k\phi_k$, the linearized system reduces to

$$\dot{z}_k(t) = (A - \rho_k D)z_k(t) + Bz_k(t-\tau), \quad k = 0, 1, 2, \ldots.$$

Substituting $z_k(t) = e^{\lambda t}q$ gives Eq (3.4). If all characteristic roots lie in the open left half-plane for every mode, the linearized delay system is exponentially stable. Then, the linearized-stability principle for semilinear parabolic delay equations then gives local asymptotic stability of E^*. If one mode has a root with positive real part, then the corresponding perturbation grows exponentially, and the equilibrium is linearly unstable. □

3.1. Delay and diffusion effects

For the positive equilibrium E^*, define the following:

$$\Delta_k(\lambda,\tau) = \det\left[\lambda I_4 + \rho_k D - A - Be^{-\lambda\tau}\right].$$

Since the delay enters only through the CTL equation, this characteristic equation can be written as

$$\Delta_k(\lambda,\tau) = P_k(\lambda) + Q_k(\lambda)e^{-\lambda\tau},$$

where P_k and Q_k are polynomials depending on A, B, D, and ρ_k.

A Hopf bifurcation may occur when $\lambda = i\omega$, $\omega > 0$, satisfies

$$P_k(i\omega) + Q_k(i\omega)e^{-i\omega\tau} = 0.$$

Equivalently,

$$|P_k(i\omega)|^2 - |Q_k(i\omega)|^2 = 0.$$

For any positive root ω_k, the corresponding critical delays are as follows:

$$\tau_{k,n} = \frac{1}{\omega_k}\left[\arg\left(-\frac{P_k(i\omega_k)}{Q_k(i\omega_k)}\right) + 2\pi n\right], \quad n = 0, 1, 2, \ldots.$$

If the transversality condition

$$\frac{d}{d\tau}\operatorname{Re}\lambda(\tau)\Big|_{\tau=\tau_{k,n}} \neq 0$$

holds, then a Hopf bifurcation occurs. The case $k = 0$ gives spatially homogeneous oscillations, while $k \geq 1$ gives spatially heterogeneous oscillatory instability.

When $\tau = 0$, the characteristic equation reduces to the following:

$$\det\left[\lambda I_4 + \rho_k D - A - B\right] = 0.$$

Equivalently, the stability of mode k is determined by the eigenvalues of $A + B - \rho_k D$. Thus diffusion modifies the stability spectrum through the spatial eigenvalues ρ_k. A diffusion-driven instability occurs if the homogeneous mode is stable but some nonzero spatial mode is unstable.

The baseline invasion indicators corresponding to Proposition 2.6 are numerically evaluated in Section 5.

4. Optimal control formulation

The reaction–diffusion delay model can be extended to an optimal-control framework in order to investigate treatment strategies that balance tumor suppression, viral administration, immune stimulation, and treatment cost.

We distinguish the continuous and discrete control problems. The continuous adjoint system and projection formulas are given as formal necessary conditions, while existence is proven for the finite-dimensional discrete optimization problem.

We introduce two bounded time-dependent control functions, $u_1(t)$ and $u_2(t)$, where $u_1(t)$ denotes the rate of oncolytic virus administration, and $u_2(t)$ denotes immune or CTL-enhancing stimulation. Time-dependent controls are suitable to represent systemic therapy, repeated intratumoral dosing, or scheduled treatment protocols. Although spatially distributed controls $u_1(x, t)$ and $u_2(x, t)$ can also be considered, the time-dependent formulation is more practical for numerical implementation and is directly compatible with the simulations presented in this work.

The controlled reaction–diffusion delay system is given by

$$\begin{cases} \dfrac{\partial S}{\partial t} = D_S \Delta S + rS\left(1 - \dfrac{S+I}{K}\right) - \beta S V - \alpha S T, \\ \dfrac{\partial I}{\partial t} = D_I \Delta I + \beta S V - \delta I - \alpha I T, \\ \dfrac{\partial V}{\partial t} = D_V \Delta V + b\delta I - \mu V + \eta_1 u_1(t), \\ \dfrac{\partial T}{\partial t} = D_T \Delta T + \dfrac{cV(x,t-\tau)T(x,t-\tau)}{1 + h_1 V(x,t-\tau) + h_2 T(x,t-\tau)} + \gamma(S+I)T - dT + \eta_2 u_2(t) T. \end{cases} \tag{4.1}$$

Here, $\eta_1 > 0$ measures the effectiveness of viral administration, while $\eta_2 > 0$ measures the effectiveness of immune stimulation. The term $\eta_1 u_1(t)$ increases the free-virus population, whereas $\eta_2 u_2(t)T$ enhances the proliferation or activity of the existing CTL population. The multiplicative immune-control term is biologically appropriate when the treatment stimulates the expansion or activation of already present CTLs. If immune-cell infusion is considered instead, an additive control term may be used.

The admissible control set is defined by the following:

$$\mathcal{U}_{ad} = \left\{(u_1, u_2) \in L^\infty(0, t_f)^2 : 0 \le u_1(t) \le u_{1,\max}, \quad 0 \le u_2(t) \le u_{2,\max}\right\}, \tag{4.2}$$

where t_f is the final treatment time. The constants $u_{1,\max}$ and $u_{2,\max}$ represent the maximum admissible viral dose and immune-stimulation intensity, respectively.

A suitable objective functional is

$$\begin{aligned} J(u_1, u_2) = &\int_0^{t_f} \int_\Omega \left[A_S S(x,t) + A_I I(x,t) + A_N(S(x,t) + I(x,t)) + \frac{A_T}{2} T^2(x,t)\right] \mathrm{d}x\, \mathrm{d}t \\ &+ \int_0^{t_f} \left[\frac{B_1}{2} u_1^2(t) + \frac{B_2}{2} u_2^2(t)\right] \mathrm{d}t + A_f \int_\Omega (S(x,t_f) + I(x,t_f))\, \mathrm{d}x. \end{aligned} \tag{4.3}$$

The terms involving A_S, A_I, and A_N penalize the persistence of uninfected tumor cells, infected tumor cells, and total tumor burden, respectively. The term $A_T T^2/2$ is not intended to penalize beneficial antitumor immunity itself; rather, it regularizes the objective and prevents the numerical optimizer from favoring unrealistically large CTL amplification. The quadratic terms involving B_1 and B_2 penalize excessive viral administration and immune stimulation. The terminal term penalizes the final total tumor burden. We assume the following:

$$A_S, A_I, A_N, A_T, A_f \ge 0, \quad B_1, B_2 > 0.$$

The optimal control problem is to find an admissible pair $(u_1^*, u_2^*) \in \mathcal{U}_{ad}$ such that

$$J(u_1^*, u_2^*) = \min_{(u_1,u_2)\in\mathcal{U}_{ad}} J(u_1, u_2), \tag{4.4}$$

subject to the controlled system (4.1), the prescribed history functions, and homogeneous Neumann boundary conditions.

4.1. Formal optimality characterization

We briefly present the formal first-order optimality conditions associated with the controlled reaction–diffusion delay system. The purpose of this subsection is not to develop an adjoint-based numerical algorithm, but rather to indicate the structure of the optimality system and to show how the projected control characterizations are obtained. Such conditions can be derived using Pontryagin's maximum principle for distributed systems with delay [26–28].

Let

$$\lambda_1(x,t), \quad \lambda_2(x,t), \quad \lambda_3(x,t), \quad \lambda_4(x,t)$$

denote the adjoint variables corresponding to

$$S(x,t), \quad I(x,t), \quad V(x,t), \quad T(x,t), \text{ respectively.}$$

For notational convenience, we write

$$V_\tau = V(x,t-\tau), \quad T_\tau = T(x,t-\tau).$$

The Hamiltonian density associated with the running cost and the reaction terms of the controlled system is given by the following:

$$\begin{aligned}\mathcal{H} = {} & A_S S + A_I I + A_N(S+I) + \frac{A_T}{2}T^2 + \frac{B_1}{2}u_1^2 + \frac{B_2}{2}u_2^2 \\ & + \lambda_1\left[rS\left(1-\frac{S+I}{K}\right) - \beta S V - \alpha S T\right] \\ & + \lambda_2\left[\beta S V - \delta I - \alpha I T\right] + \lambda_3\left[b\delta I - \mu V + \eta_1 u_1\right] \\ & + \lambda_4\left[\frac{c V_\tau T_\tau}{1 + h_1 V_\tau + h_2 T_\tau} + \gamma(S+I)T - dT + \eta_2 u_2 T\right].\end{aligned} \tag{4.5}$$

Formally, the full adjoint system is obtained by differentiating the spatially integrated Hamiltonian with respect to the state variables and by including the adjoint diffusion operators. The adjoint equations are solved backward in time and are supplemented with terminal conditions induced by the terminal tumor-burden penalty

$$A_f \int_\Omega \left(S(x,t_f) + I(x,t_f)\right) \mathrm{d}x.$$

Thus, the terminal conditions are

$$\lambda_1(x,t_f) = A_f, \quad \lambda_2(x,t_f) = A_f, \quad \lambda_3(x,t_f) = 0, \quad \lambda_4(x,t_f) = 0.$$

Because the state system contains the delayed immune-activation term, the adjoint equations also contain advanced contributions. These terms arise because variations of $V(x,t)$ and $T(x,t)$ affect the delayed immune-response term at the later time $t+\tau$. Consequently, advanced terms appear on the interval $0 \le t \le t_f - \tau$, whereas these delay-induced contributions vanish for $t_f - \tau < t \le t_f$. This feature is one of the main technical complications in adjoint-based numerical methods for delayed optimal-control problems.

Proposition 4.1 (Formal control characterization)**.** *Suppose that an optimal pair and the associated adjoint variables exist and satisfy the first-order necessary conditions. Then,*

$$u_1^*(t) = \Pi_{[0,u_{1,\max}]}\left(-\frac{\eta_1}{B_1}\int_\Omega \lambda_3(x,t)\ \mathrm{d}x\right), \tag{4.6}$$

and

$$u_2^*(t) = \Pi_{[0,u_{2,\max}]}\left(-\frac{\eta_2}{B_2}\int_\Omega \lambda_4(x,t)T(x,t)\ \mathrm{d}x\right). \tag{4.7}$$

Proof. Differentiating the spatially integrated Hamiltonian with respect to the spatially uniform controls gives the following:

$$B_1u_1(t) + \eta_1\int_\Omega \lambda_3(x,t)\ \mathrm{d}x = 0, \quad B_2u_2(t) + \eta_2\int_\Omega \lambda_4(x,t)T(x,t)\ \mathrm{d}x = 0.$$

Projecting these unconstrained critical controls onto their admissible intervals yields (4.6) and (4.7). □

These projection formulas have a natural interpretation. The viral-administration control $u_1^*(t)$ is governed by the spatial integral of the adjoint variable λ_3, which measures the marginal effect of increasing the free-virus population on the objective functional. The immune-stimulation control $u_2^*(t)$ depends on the weighted quantity $\lambda_4 T$, reflecting the fact that u_2 multiplicatively acts on the CTL population. Thus, immune stimulation is favored at times when CTLs are present and when increasing the CTL activity decreases the objective.

The formal optimality system is included to describe the first-order structure of the continuous control problem, but it is not used in the computations. Because the delay produces advanced terms at $t + \tau$ in the adjoint equations, a standard forward–backward sweep would require future-state information and additional interpolation during backward integration. Therefore, we use the direct finite-dimensional optimization method described below. This approach avoids solving an adjoint reaction–diffusion system with advanced terms and permits direct enforcement of the control bounds. The projection formulas provide analytical interpretation, whereas the reported schedules are numerically computed using a constrained routine such as `fmincon`.

4.2. Semi-discrete formulation for numerical computation

To numerically implement the optimal-control problem, we first discretize the spatial domain into N_x grid points. Let

$$S_j(t), \quad I_j(t), \quad V_j(t), \quad T_j(t), \quad j = 1, 2, \ldots, N_x,$$

denote the finite-difference approximations of the uninfected tumor cells, infected tumor cells, free virus particles, and CTL population, respectively. We denote by L_N the finite-difference matrix corresponding to the Laplacian operator subject to homogeneous Neumann boundary condition. Thus, L_N incorporates the zero-flux boundary conditions at the endpoints of the computational domain.

Writing

$$S(t) = (S_1(t), \ldots, S_{N_x}(t))^\top, \quad I(t) = (I_1(t), \ldots, I_{N_x}(t))^\top,$$

and similarly for $V(t)$ and $T(t)$, the semi-discrete controlled system can be expressed in vector form as

$$\begin{cases} \dot{S} = D_S L_N S + rS \circ \left(\mathbf{1} - \dfrac{S+I}{K}\right) - \beta S \circ V - \alpha S \circ T, \\ \dot{I} = D_I L_N I + \beta S \circ V - \delta I - \alpha I \circ T, \\ \dot{V} = D_V L_N V + b\delta I - \mu V + \eta_1 u_1(t)\mathbf{1}, \\ \dot{T} = D_T L_N T + \mathcal{G}(V_\tau, T_\tau) + \gamma(S+I) \circ T - dT + \eta_2 u_2(t) T. \end{cases} \tag{4.8}$$

Here $\circ$ denotes componentwise multiplication, $\mathbf{1} \in \mathbb{R}^{N_x}$ is the vector of ones, and $V_\tau = V(t-\tau)$, $T_\tau = T(t-\tau)$. The delayed immune-activation term is given by

$$\mathcal{G}(V_\tau, T_\tau) = \frac{c\, V(t-\tau) \circ T(t-\tau)}{\mathbf{1} + h_1 V(t-\tau) + h_2 T(t-\tau)}. \tag{4.9}$$

The division in (4.9) is understood componentwise.

For a prescribed admissible control pair (u_1, u_2), system (4.8) is a finite-dimensional system of delay differential equations. The required history functions are obtained by evaluating the prescribed initial spatial histories at the grid points.

For the numerical optimization, the controls are approximated by piecewise-constant functions over N_c treatment intervals, that is,

$$u_1(t) = u_{1,k}, \quad u_2(t) = u_{2,k}, \quad t \in [t_k, t_{k+1}), \quad k = 1, 2, \ldots, N_c.$$

The unknown control parameters are collected into the finite-dimensional vector

$$\mathbf{u} = (u_{1,1}, \ldots, u_{1,N_c}, u_{2,1}, \ldots, u_{2,N_c})^\top.$$

The bound constraints on the continuous controls are imposed directly on the components of $\mathbf{u}$, namely

$$0 \le u_{1,k} \le u_{1,\max}, \quad 0 \le u_{2,k} \le u_{2,\max}, \quad k = 1, \ldots, N_c.$$

For each trial vector $\mathbf{u}$, the semi-discrete delay system is solved forward in time, and the corresponding discrete objective functional is evaluated. A convenient quadrature-based approximation of the objective functional is

$$\begin{aligned} J_h(\mathbf{u}) = &\sum_{m=1}^{N_t} \Delta t\, \Delta x \sum_{j=1}^{N_x} \left[A_S S_j^m + A_I I_j^m + A_N (S_j^m + I_j^m) + \frac{A_T}{2} (T_j^m)^2 \right] \\ &+ \sum_{m=1}^{N_t} \Delta t \left[\frac{B_1}{2} (u_1^m)^2 + \frac{B_2}{2} (u_2^m)^2 \right] + A_f \Delta x \sum_{j=1}^{N_x} (S_j^{N_t} + I_j^{N_t}). \end{aligned} \tag{4.10}$$

Here S_j^m, I_j^m, V_j^m, and T_j^m denote the numerical approximations at the spatial grid point x_j and time level t_m. The quantities u_1^m and u_2^m denote the values of the piecewise-constant controls at time t_m.

Proposition 4.2 (Existence of a discrete optimal control)**.** *Let $U_h \subset \mathbb{R}^{2N_c}$ be the set of piecewise-constant control vectors satisfying the bounds above. Assume that the semi-discrete state system has a unique solution for every $\mathbf{u} \in U_h$ and that J_h is continuous on U_h. Then there exists $\mathbf{u}_h^* \in U_h$ such that*

$$J_h(\mathbf{u}_h^*) = \min_{\mathbf{u} \in U_h} J_h(\mathbf{u}).$$

Proof. The set U_h is nonempty and compact in the finite-dimensional space $\mathbb{R}^{2N_c}$. The conclusion follows from continuity of J_h and the Weierstrass theorem. □

Then, the resulting finite-dimensional constrained optimization problem is then solved using a bounded nonlinear programming routine. This direct optimization approach is particularly convenient for the present delay reaction–diffusion system because it avoids the need to solve the adjoint system, which contains advanced delay terms and is more delicate to numerically implemented.

The computational procedure is summarized as follows:

1) Set t_f, N_x, N_t, and N_c, and specify the parameters, control bounds, and nonnegative histories;
2) Initialize the control vector $\mathbf{u}^{(0)}$;
3) For each control iterate, solve (4.8) forward in time and compute $J_h(\mathbf{u})$;
4) Update $\mathbf{u}$ using a constrained optimization routine;
5) Repeat until the prescribed stopping criterion is satisfied.

5. Numerical simulations

This section presents numerical simulations illustrating the qualitative behavior of the reaction–diffusion delay model and its optimal-control extension. The computations were performed in one spatial dimension on the scaled domain $\Omega = (0, 1)$. The spatial derivatives were approximated by second-order finite differences with homogeneous Neumann boundary conditions, and the resulting finite-dimensional delay differential system was solved using MATLAB's `dde23` solver.

The simulations are intended to illustrate representative tumor–virus–immune dynamics, spatial heterogeneity, delayed immune activation, and the potential benefit of treatment optimization. Therefore, they should therefore be interpreted as illustrative examples for the selected parameter set, rather than as a complete parameter-sensitivity or bifurcation study.

All statements in this section are numerical observations for the specified discretization, histories, and parameter set; they are not general analytical conclusions. Mathematically established results are confined to the propositions and theorems in Sections 2–4.

Unless otherwise stated, the history functions are taken to be independent of the delay variable $\theta \in [-\tau, 0]$. The initial profile consists of a relatively high uninfected tumor population, a localized infected-cell population near the center of the domain, a localized viral inoculum, and a weakly distributed CTL population. Specifically, the initial histories, for $-\tau \le \theta \le 0$, are

$$S(x,\theta) = 0.75,\ I(x,\theta) = 0.04e^{-90(x-0.5)^2},\ V(x,\theta) = 0.12e^{-90(x-0.5)^2},\ T(x,\theta) = 0.08 + 0.02\cos(\pi x).$$

This choice represents localized viral administration into a tumor region and allows the model to capture local infection, viral spread, and the subsequent immune response.

Figure 3 shows the initial spatial profiles used in all numerical simulations.

The baseline parameter values used in the simulations are listed in Table 2. The numerical settings for the direct optimal-control computations are summarized in Table 3. The simulations are performed in scaled variables; in particular, the logistic growth term is implemented with the scaled carrying capacity $K = 1$.

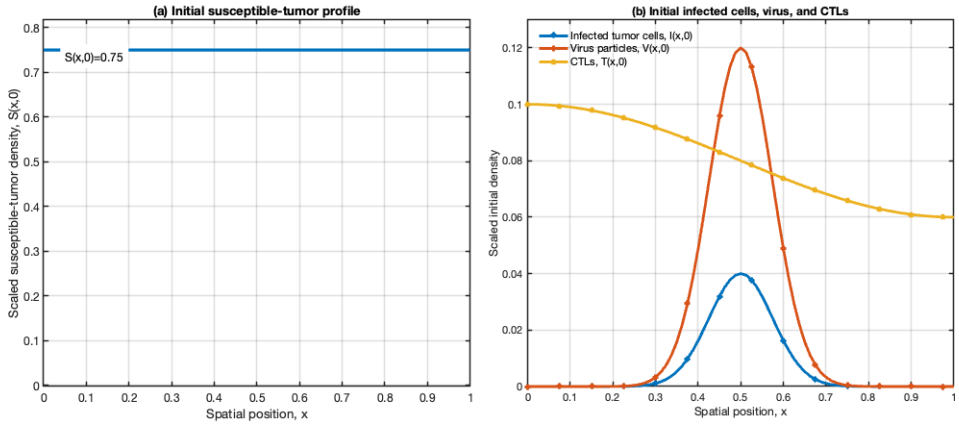

Figure 3. Initial spatial profiles on $\Omega = (0, 1)$. Panel (a) shows the uniform susceptible-tumor profile $S(x, 0) = 0.75$. Panel (b) shows the localized infected-cell and virus profiles together with the initial CTL distribution.

The values in Table 2 are scaled, illustrative choices informed by related tumor–virus–immune models [11, 18, 20]. They are not patient-specific estimates. Where direct experimental estimates are unavailable, values are selected to produce biologically plausible dynamics and to satisfy the sufficient assumptions of Theorem 2.3.

Table 2. Baseline scaled parameter values used in the numerical simulations, with source or modeling justification.

Parameter	Value	Description	Source or justification
D_S	2.0×10^{-4}	Diffusion coefficient of uninfected tumor cells	Scaled illustrative value
D_I	2.0×10^{-4}	Diffusion coefficient of infected tumor cells	Set equal to D_S; Theorem 2.3
D_V	4.0×10^{-3}	Diffusion coefficient of virus particles	Scaled illustrative value
D_T	2.5×10^{-3}	Diffusion coefficient of CTLs	Scaled illustrative value
r	0.18	Intrinsic tumor growth rate	Scaled illustrative value
K	1	Scaled tumor carrying capacity	Nondimensional normalization
β	0.85	Infection rate of tumor cells by virus particles	Informed by [11, 20]
α	0.55	Immune-mediated tumor-cell killing rate	Informed by [11]
δ	0.18	Lysis rate of infected tumor cells	Scaled illustrative value
b	1.60	Viral burst size	Scaled illustrative value
μ	0.75	Virus clearance rate	Scaled illustrative value
c	0.70	Maximum virus-induced CTL activation rate	Informed by [11]
h_1	0.40	Saturation parameter for viral stimulation	Model assumption
h_2	0.55	CTL competition/saturation parameter	Model assumption; Theorem 2.3
γ	0.30	Tumor-induced CTL stimulation rate	Scaled illustrative value
d	0.42	CTL clearance rate	Chosen so $d > \gamma K$
τ	5.0	Immune activation delay	Illustrative delayed-response scale

To relate the analytical thresholds in Section 3 to the simulations, we evaluate the main invasion indicators using the baseline parameters in Table 2; see Figure 4. Since $\mathcal{R}_0 > 1$, the virus can invade E_1.

At E_2, CTL activation is below clearance, so CTL invasion is not supported. Moreover, $d/(\gamma K) > 1$, so E_3 is not biologically feasible for the baseline parameter set. Thus, the baseline dynamics lie in a virus-driven regime.

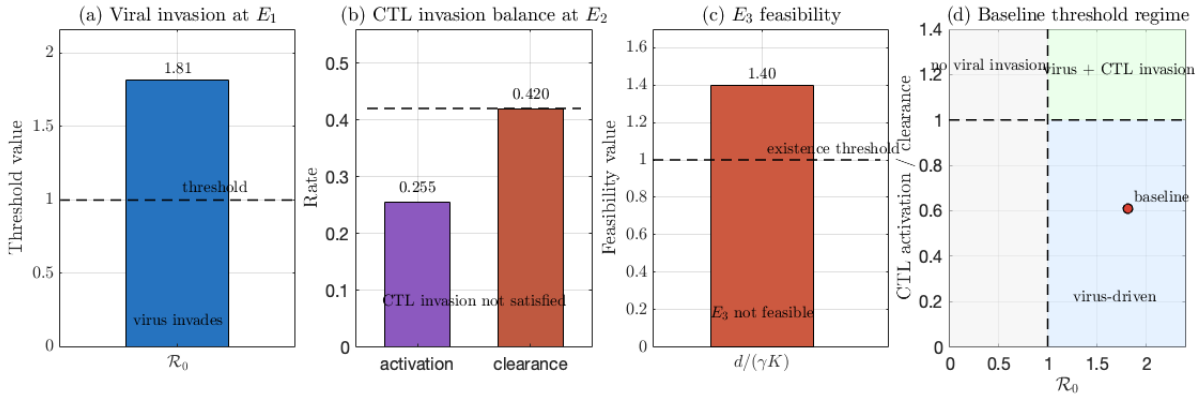

Figure 4. Threshold diagnostics computed from the scaled baseline parameters in Table 2. Panels (a)–(d) show viral invasion at E_1, the CTL invasion balance at E_2, feasibility of E_3, and the location of the baseline point in the threshold plane.

Table 3. Numerical settings for the optimal-control simulations.

Quantity	Value
Domain and final time	$\Omega = (0, 1), \quad t_f = 40$
Discretization	$N_x = 31, \quad N_t = 120, \quad N_c = 8$
Mesh sizes	$\Delta x = 1/30, \quad \Delta t = 40/119$
Control bounds	$0 \le u_1(t), u_2(t) \le 1$
Control effectiveness	$\eta_1 = 0.55, \quad \eta_2 = 0.45$
State weights	$A_S = 1.0,\ A_I = 1.2,\ A_N = 0.8,\ A_T = 0.10,\ A_f = 8.0$
Control weights	$B_1 = 0.20, \quad B_2 = 0.25$
Tolerances	$\texttt{RelTol} = 10^{-3}, \quad \texttt{AbsTol} = 10^{-5}$

The uncontrolled simulations in Figures 5 and 6 are shown on $0 \le t \le 60$, while the optimal-control simulations use $t_f = 40$, as reported in Table 3. The controls are approximated by $N_c = 8$ piecewise-constant values on $[0, t_f]$. For each trial control vector, the semi-discrete delay system is solved forward in time, the discrete objective functional is evaluated, and the control vector is updated using `fmincon` subject to the prescribed bounds. Unless otherwise stated, the initial control guess is the constant schedule $u_1(t) = u_2(t) = 0.5$, the controls are held constant on each of the N_c treatment intervals, delayed states are evaluated by the interpolation used internally by `dde23`, and the optimization is stopped when successive changes in the objective and in the control vector satisfy the default tolerance criteria of the constrained optimizer. Because the resulting problem is nonconvex, the computed control should be interpreted as a locally optimal schedule for the chosen discretization and initial guess.

The jumps in the displayed controls arise from the piecewise-constant parameterization over $N_c = 8$ treatment intervals. They are numerical features of the chosen control discretization rather than discontinuities imposed by the biological model.

Figure 5 summarizes the uncontrolled dynamics. The average uninfected tumor population decreases

over time, while the infected-cell population initially increases as susceptible tumor cells become infected. The total tumor burden also decreases, reflecting the combined effects of viral infection, infected-cell lysis, and immune-mediated killing. The virus curve shows viral amplification followed by clearance, whereas the CTL curve displays a delayed immune response. The heatmaps show that both tumor burden and virus density remain spatially heterogeneous, demonstrating the importance of the reaction–diffusion formulation.

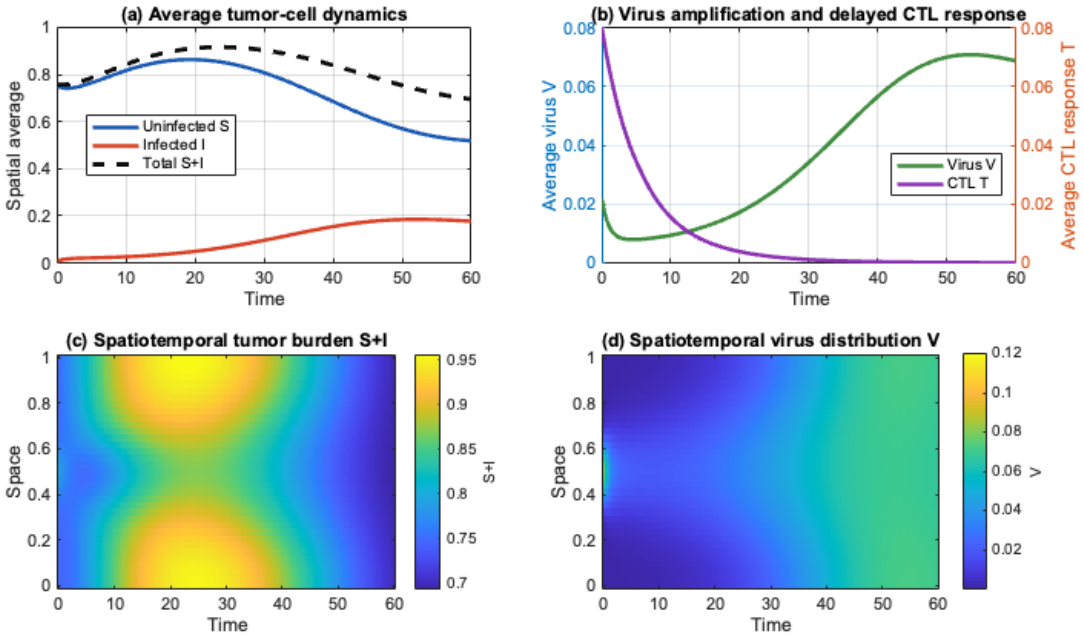

Figure 5. Spatiotemporal dynamics without control on $\Omega = (0, 1)$ for $0 \le t \le 60$, using the histories stated in Section 5, the scaled parameters in Table 2, and homogeneous Neumann boundary conditions. The upper panels show spatial averages; the lower panels show total tumor burden and virus density.

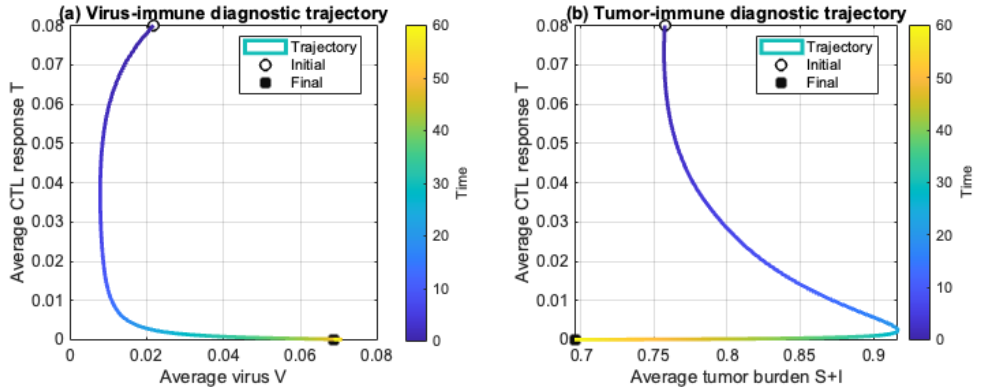

Figure 6. Time-colored phase-plane diagnostics for the uncontrolled simulation on $\Omega = (0, 1)$, $0 \le t \le 60$, using Table 2. Panel (a) shows average virus density versus average CTL response; panel (b) shows average tumor burden versus average CTL response.

Figure 6 presents time-colored phase-plane diagnostics for the uncontrolled model. The trajectories show that the CTL response does not instantaneously follow viral expansion or tumor decline, thus reflecting the delayed and nonlinear immune-activation mechanism. These plots are qualitative diagnostics and should not be interpreted as a bifurcation analysis.

Next, we consider the optimal-control simulations. The direct optimization method avoids solving the delayed adjoint system and imposes the control bounds directly on the finite-dimensional optimization variables.

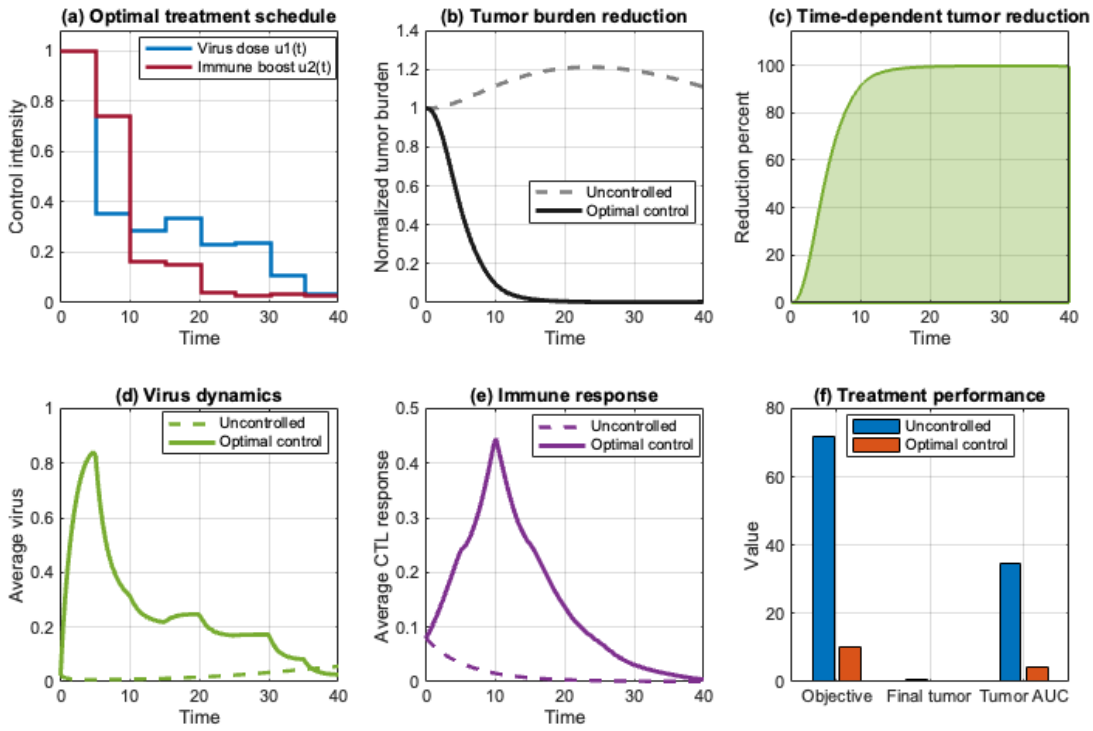

Figure 7. Locally optimal numerical-control simulation on $\Omega = (0, 1)$ for $0 \le t \le 40$, using the baseline parameters in Table 2, $N_c = 8$ piecewise-constant intervals, and the single initial guess $u_1(t) = u_2(t) = 0.5$. The finite-dimensional problem is nonconvex, so global optimality is not claimed.

Figure 7 summarizes the effect of the computed locally optimal numerical treatment strategy. The computed control profiles indicate the treatment intervals favored by the local optimizer. The controlled tumor burden is lower than the uncontrolled tumor burden, and the percentage-reduction panel quantifies the improvement obtained through treatment. The virus and CTL panels show that the computed strategy modifies both therapeutic virus dynamics and the immune response. The performance panel compares the objective value, final tumor burden, and cumulative tumor burden, showing that the controlled strategy improves treatment outcome for the chosen parameter set.

Figure 8 illustrates the spatial effect of the computed locally optimal numerical strategy. Compared with the uncontrolled case, the controlled tumor burden is reduced throughout the spatial domain. The spatial-reduction panel identifies where the treatment effect is strongest. The controlled virus

and CTL heatmaps show how the treatment schedule shapes the spatial and temporal distributions of the therapeutic virus and immune response. These results suggest that the computed locally optimal treatment schedule can improve tumor suppression not only in spatial averages but also across the tumor region.

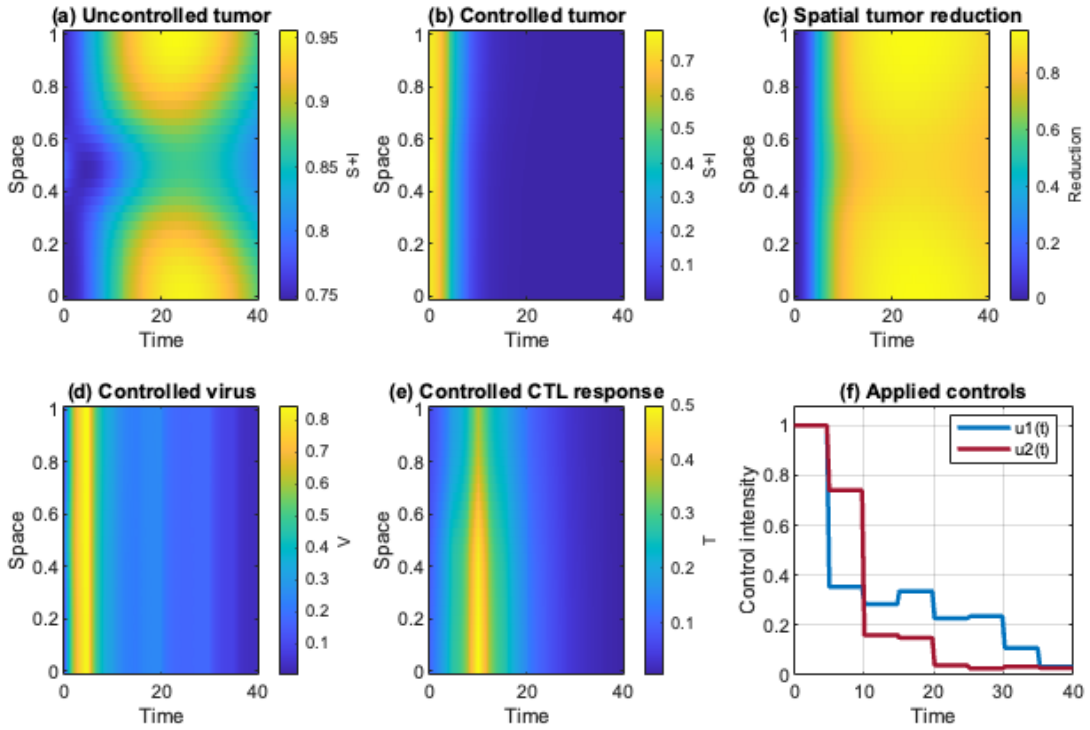

Figure 8. Spatiotemporal comparison on $\Omega = (0, 1)$, $0 \le t \le 40$, using Tables 2 and 3. Panels (a) and (b) should be read using their displayed tumor-burden scales; the virus, CTL, and reduction panels use variable-specific color bars, so colors should not be compared directly across different quantities.

Figure 9 shows the components of the objective functional. The treatment-cost panel reflects the penalty associated with applying the viral and immune controls. With the revised objective functional, the state contribution penalizes tumor burden and excessive CTL amplification rather than rewarding CTLs linearly. The cost-decomposition panel separates the total objective into state, control, and terminal contributions, illustrating the trade-off between tumor reduction, immune regularization, and treatment intensity.

Effect of the immune-response delay We compare the uncontrolled system for $\tau = 0, 5, 10$, and 15, while keeping all other parameters and history functions fixed at the baseline values in Table 2. The delay simulations use $N_x = 81$, 2000 output points, RelTol $= 10^{-8}$, and AbsTol $= 10^{-10}$, which differ from the optimal-control settings in Table 3. Figure 10 shows the normalized spatially averaged tumor burden and CTL response, together with their percentage differences relative to the no-delay case. Increasing τ delays CTL activation and alters the transient tumor–immune dynamics. These results provide a numerical sensitivity illustration rather than a complete delay-bifurcation analysis.

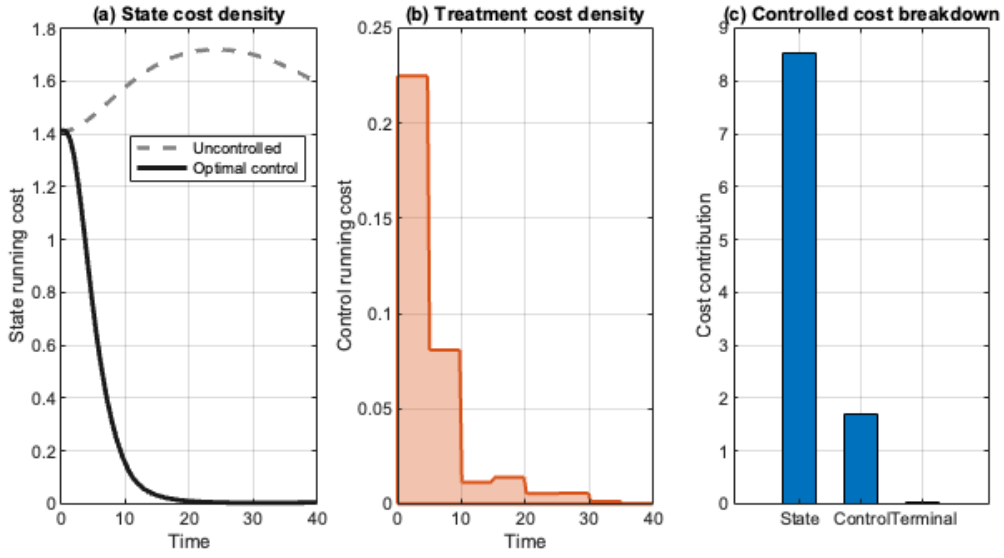

Figure 9. Objective-functional components for the optimal-control simulation on $0 \le t \le 40$, using Tables 2 and 3. The panels show the state running contribution, treatment cost, and state, control, and terminal contributions.

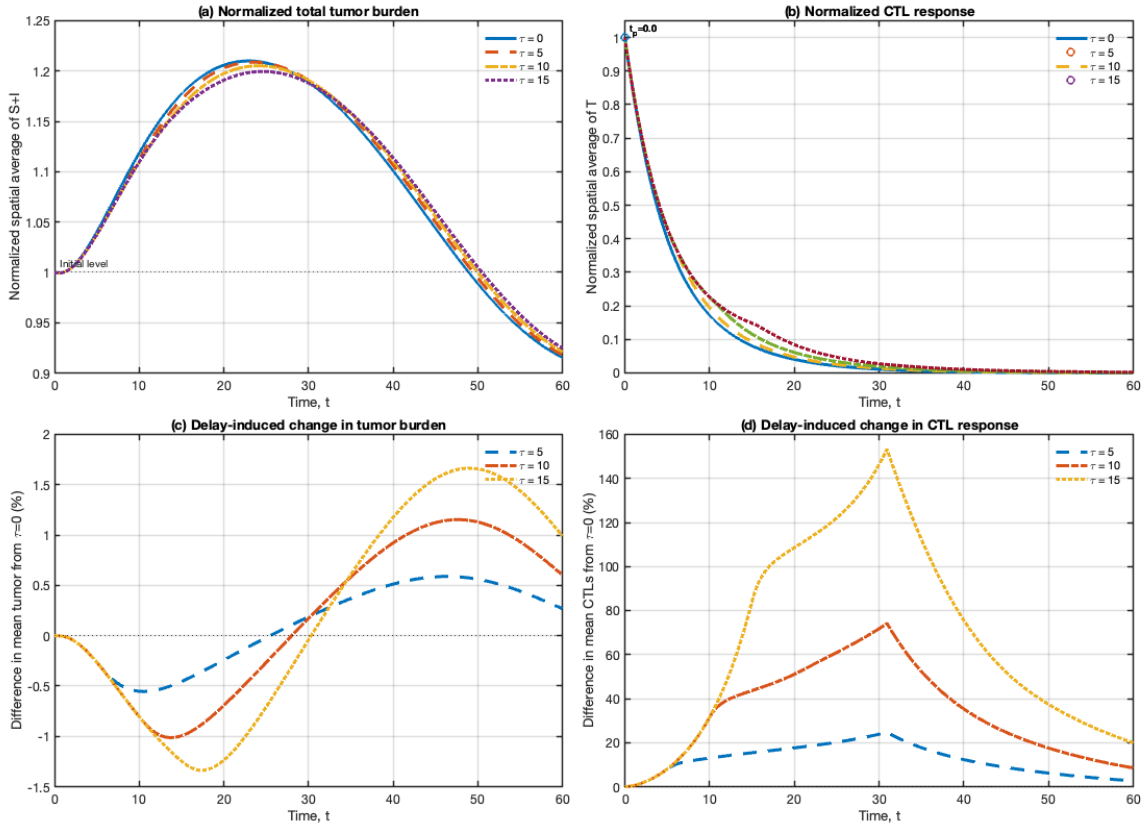

Figure 10. Effect of the immune-response delay for $\tau = 0, 5, 10$, and 15. Panels (a) and (b) show normalized mean tumor burden and CTL response, while panels (c) and (d) show percentage differences relative to $\tau = 0$.

6. Discussion

The proposed model integrates direct viral oncolysis, immune-mediated tumor killing, spatial diffusion, and delayed CTL activation within a single tumor–virus–immune framework. The simulations indicate that tumor burden, viral spread, and immune responses may remain spatially heterogeneous, suggesting that spatially averaged models can miss important local treatment effects.

The equilibrium and modal stability analyses connect the spatial model with its temporal counterpart. Although spatially homogeneous equilibria coincide with those of the corresponding delay system, diffusion introduces additional spatial modes that may alter stability. The numerical results further indicate that spatial diffusion, immune-response delay, and treatment scheduling shape the transient tumor–virus–immune dynamics. For the selected parameter set, the computed locally optimal viral-administration and immune-stimulation schedules reduce tumor burden under treatment-cost constraints.

Several limitations remain. Diffusion provides only a simplified description of movement within tumor tissue, the immune response is represented by a single CTL population, and the model assumes constant parameters and spatially uniform controls.

The global boundedness result is established only under the sufficient conditions $D_S = D_I$, $h_2 > 0$, and $d > \gamma M_N$. Moreover, the treatment outcomes in Section 5 are numerical observations for a scaled illustrative parameter set and should not be interpreted as general analytical results or patient-specific predictions.

7. Conclusions

This paper developed a reaction–diffusion delay model for tumor virotherapy with virus-induced CTL activation. The analysis establishes positivity, local well-posedness, global boundedness under explicit sufficient conditions, spatially homogeneous equilibria, and a modal stability framework. Numerical simulations illustrate the effects of spatial heterogeneity, immune-response delay, and locally optimal treatment schedules for the selected parameter set.

The model provides a tractable basis for further analytical, computational, and data-driven studies of spatial tumor virotherapy. Future work will consider broader boundedness conditions, parameter estimation, sensitivity and bifurcation analyses, spatially distributed controls, and experimental validation.

Use of AI tools declaration

The authors declare they have not used Artificial Intelligence (AI) tools in the creation of this article.

Acknowledgments

The author would like to thank the Editor and the anonymous reviewers for their valuable and constructive comments, which helped improve the quality and clarity of the manuscript.

Conflict of interest

The author declares no conflict of interest.

References

1. S. J. Russell, K. W. Peng, J. C. Bell, Oncolytic virotherapy, *Nat. Biotechnol.*, **30** (2012), 658–670. https://doi.org/10.1038/nbt.2287
2. J. C. Bell, S. H. Lichty, B. D. Stojdl, Getting oncolytic virus therapies off the ground, *Cancer Cell*, **4** (2003), 7–11. https://doi.org/10.1016/s1535-6108(03)00170-3
3. N. Macedo, J. T. Miller, J. Haq, D. Kaufman, Clinical landscape of oncolytic virus research in 2020, *J. ImmunoTher. Cancer*, **8** (2003), e001486. https://doi.org/10.1136/jitc-2020-001486
4. D. Xiao, H. Zhang, Y. Liu, Y. Li, G. Li, Y. Ning, Oncolytic viruses: advanced strategies in cancer therapy, *Signal Transduction Targeted Ther.*, **11** (2026), 45. https://doi.org/10.1038/s41392-025-02343-3
5. R. J. Prestwich, K. J. Harrington, H. S. Pandha, R. G. Vile, A. A. Melcher, F. Errington, Oncolytic viruses: a novel form of immunotherapy, *Expert Rev. Anticancer Ther.*, **8** (2008), 1581–1588. https://doi.org/10.1586/14737140.8.10.1581
6. D. K. Bhatt, T. Daemen, Molecular circuits of immune sensing and response to oncolytic virotherapy, *Int. J. Mol. Sci.*, **25** (2024), 4691. https://doi.org/10.3390/ijms25094691
7. C. F. Kollmann, N. van Montfoort, P. Cordelier, J. Pol, D. Olagnier, Oncolytic virotherapy: sparking durable anti-tumor immunity through microenvironment modulation, *Semin. Immunol.*, **80** (2025), 101994. https://doi.org/10.1016/j.smim.2025.101994
8. D. Wodarz, Viruses as antitumor weapons: defining conditions for tumor remission, *Cancer Res.*, **61** (2001), 3501–3507.
9. A. Friedman, J. P. Tian, G. Fulci, E. A. Chiocca, J. Wang, Glioma virotherapy: effects of innate immune suppression and increased viral replication capacity, *Cancer Res.*, **66** (2006), 2314–2319. https://doi.org/10.1158/0008-5472.CAN-05-2661
10. L. R. Paiva, C. Binny, S. C. Ferreira Jr., M. L. Martins, A multiscale mathematical model for oncolytic virotherapy, *Cancer Res.*, **69** (2009), 1205–1211. https://doi.org/10.1158/0008-5472.CAN-08-2173
11. Q. Li, Y. Xiao, Modeling the virus-induced tumor-specific immune response with delay in tumor virotherapy, *Commun. Nonlinear Sci. Numer. Simul.*, **108** (2022), 106196. https://doi.org/10.1016/j.cnsns.2021.106196
12. F. A. Rihan, *Delay Differential Equations and Applications to Biology*, Forum for Interdisciplinary Mathematics, Springer, Cham, 2nd edition, 2026. https://doi.org/10.1007/978-3-032-08645-7
13. F. A. Rihan, Modeling virus–tumor interactions and control in oncolytic virotherapy, in *Bioinformatics and Computational Biology*, volume 2977 of *Communications in Computer and Information Science*, Springer, Cham, 2026. https://doi.org/10.1007/978-3-032-26028-4_1

14. D. Morselli, M. E. Delitala, F. Frascoli, Agent-based and continuum models for spatial dynamics of infection by oncolytic viruses, *Bull. Math. Biol.*, **85** (2023), 92. https://doi.org/10.1007/s11538-023-01192-x
15. G. E. Mahlbacher, K. C. Reihmer, H. B. Frieboes, Mathematical modeling of tumor-immune cell interactions, *J. Theor. Biol.*, **469** (2019), 47–60. https://doi.org/10.1016/j.jtbi.2019.03.002
16. S. Marzban, S. Srivastava, S. Kartika, R. Bravo, R. Safriel, A. Zarski, et al., Spatial interactions modulate tumor growth and immune infiltration, *npj Syst. Biol. Appl.*, **10** (2024), 106. https://doi.org/10.1038/s41540-024-00438-1
17. S. Hussain, M. Sen, V. Volpert, Infection spreading in tissue as a reaction-diffusion wave, *Math. Med. Biol.*, **41** (2024), 169–191. https://doi.org/10.1093/imammb/dqae009
18. M. El Younoussi, Z. Hajhouji, K. Hattaf, N. Yousfi, Dynamics of a reaction–diffusion fractional-order model for m1 oncolytic virotherapy with ctl immune response, *Chaos, Solitons Fractals*, **157** (2022), 111957. https://doi.org/10.1016/j.chaos.2022.111957
19. M. El Younoussi, Z. Hajhouji, K. Hattaf, N. Yousfi, A reaction–diffusion fractional model for cancer virotherapy with immune response and Hattaf time-fractional derivative, in *Trends in Biomathematics: Modeling Epidemiological, Neuronal, and Social Dynamics* (eds. R. P. Mondaini), Springer, Cham, 2023. https://doi.org/10.1007/978-3-031-33050-6_7
20. Z. Wang, Modeling oncolytic virus therapy with distributed delay and nonlocal diffusion, *Adv. Contin. Discrete Models*, **2024** (2024), 59. https://doi.org/10.1186/s13662-024-03859-8
21. D. K. Bhatt, T. Janzen, T. Daemen, F. J. Weissing, Effects of virus-induced immunogenic cues on oncolytic virotherapy, *Sci. Rep.*, **14** (2024), 28861. https://doi.org/10.1038/s41598-024-80542-8
22. S. Omer, H. Mambili-Mamboundou, Assessing the impact of immunotherapy on oncolytic virotherapy in the treatment of cancer, *J. Appl. Math. Comput.*, **70** (2024), 4793–4825. https://doi.org/10.1007/s12190-024-02139-8
23. K. R. Fister, J. H. Donnelly, Immunotherapy: an optimal control theory approach, *Math. Biosci. Eng.*, **2** (2005), 499–510. https://doi.org/10.3934/mbe.2005.2.499
24. D. Henry, *Geometric Theory of Semilinear Parabolic Equations*, Springer, Berlin, 1981.
25. A. Pazy, *Semigroups of Linear Operators and Applications to Partial Differential Equations*, Springer, New York, 1983.
26. J. K. Hale, S. M. V. Lunel, *Introduction to Functional Differential Equations*, Springer, New York, 1993.
27. H. L. Smith, *An Introduction to Delay Differential Equations with Applications to the Life Sciences*, Springer, New York, 2011.
28. S. Lenhart, J. T. Workman, *Optimal Control Applied to Biological Models*, Chapman & Hall/CRC, Boca Raton, 2007.

AIMS Press